Short- and intermediate-range order in molten metal tribromides: a computer simulation study

2000 J. Phys.: Condens. Matter 12 10389

(http://iopscience.iop.org/0953-8984/12/50/303)

J. Phys.: Condens. Matter **12** (2000) 10389–10410. Printed in the UK PII: S0953-8984(00)15772-8

Short- and intermediate-range order in molten metal tribromides: a computer simulation study

Francis Hutchinson, Mark Wilson and Paul A Madden

Physical and Theoretical Chemistry Laboratory, Oxford University, South Parks Road, Oxford OX1 3QZ, UK

Received 25 July 2000

Abstract. Molecular dynamics simulation studies were performed on four molten metal tribromides, MBr_3, M = La, Ce, Y, Dy. The many-body (polarizable-ion) simulation potentials were constructed from recent metal trichloride potentials using physically transparent scaling arguments to account to the change in anion size and polarizability. Comparison was made with neutron scattering results by constructing the total structure factors from the simulated partial functions. In addition, difference functions, which exploit the proposed isomorphous nature of the (Dy, Y) and (La, Ce) pairs, are constructed and compared with experiment. The structural comparison between different trihalide materials is further extended by producing model structure factors, obtained by re-weighting and scaling the simulated partial structure factors for the tribromides, which are then compared with experimental structure factors for certain trichlorides and tri-iodides. Strong structural similarities are demonstrated between the different halides with similar cation–anion radius ratios. It is further suggested that the structures exhibited by the trihalides fall into a small number of characteristic structure classes. The short- and intermediate-range order within the different structure classes is then exemplified by analysis of the local coordination environments and the connectivity of the coordination polyhedra.

1. Introduction

The investigation of metal chlorides has tended to dominate both experimental and theoretical work on the properties of molten metal halides [1, 2]. In experimental terms, molten chlorides are generally easier to prepare than the fluoride, bromide or iodide analogues. The fluorides have significantly higher melting points and are very corrosive. The bromides and iodides are relatively susceptible to decomposition at the high temperatures required for the study of the molten state. The trivalent metal halides are a particularly interesting class of materials on which to examine liquid structure, since a wide range of cation radii may be scanned, from La^{3+} ($\sigma \sim 1.4$ Å) to Al^{3+} ($\sigma \sim 0.8$ Å), with a commensurate change in liquid state properties. Within the chlorides, $LaCl_3$ is an ionic melt, whereas $AlCl_3$ is a molecular liquid, and intermediate cation-sized systems (e.g. YCl_3) form networks. Recently, a systematic investigation of the structures of the trivalent metal chlorides has been made by neutron scattering methods [3–6]. Simulation studies were also performed in parallel with the experimental investigation [7–9]. The simulation studies show that the range of behaviour exhibited by the chlorides may be accounted for with a generic, formal-charge *ionic* interaction model in which the changes in potential parameters, which distinguish one MCl_3 system from another, are derived solely from the differences in the cation radius. The work focuses attention on the role of anion polarization effects, which determine how local coordination polyhedra (MCl_6^{3-} etc) are linked together in the melt [10], and thereby strongly affect the structure on intermediate length scales.

0953-8984/00/5010389+22$30.00

In addition to the trichlorides, neutron scattering experiments have now been carried out on a range of tribromides and tri-iodides [3,11,12]. There are two main themes to the extension of the simulation work to encompass these systems. Firstly, it is of interest to see whether the 'generic' model can be generalized to allow for a change in *anionic* properties by simply changing potential parameters related to the anion radius and polarizability. Secondly, an examination of the bromides will broaden the insights into the structures which have been gained on the chloride systems. The simulation studies complement the experiments in providing real-space structures, since the experimental measurements are primarily of total structure factors.

In the chlorides the decrease in cation size is accompanied by changes in coordination number—this does not occur continuously with the ratio of cation to anion radii; rather it occurs in steps. This is a familiar situation for *crystal* structures, where the requirement of long-range order means that only certain coordination numbers are observed, but is less clearly a necessary condition for a liquid. In the trivalent metal halides, there are two main crystal structure types. The UCl_3 is nine-coordinate and, in the chlorides, is adopted by the large cations like La^{3+} and Ce^{3+} (with ionic radii, $\sigma_+ \sim 1.4$ Å, giving a cation:anion radius ratio ρ_{+-} of ∼0.83). When these systems melt, they appear to retain a high coordination number of 7–8. The six-coordinate YCl_3 (or BiI_3, which differs only in the stacking sequence of the close-packed anions) structure is adopted by a very broad class of smaller cations, ranging from Dy^{3+} ($\sigma_+ \sim 1.25$ Å, $\rho_{+-} = 0.72$) to Al^{3+} ($\sigma_+ \sim 0.9$ Å, $\rho_{+-} = 0.53$). On melting, the larger cations of this class (larger than Sc^{3+}, $\sigma_+ \sim 1.12$ Å, $\rho_{+-} = 0.66$) remain roughly six-coordinate, whereas the smaller ones (Al^{3+} and Fe^{3+}) relax to tetrahedral coordination—with interesting consequences for the phase behaviour [13]. Within each step, of roughly constant coordination number and therefore of very similar structure at the nearest-neighbour level, a range of liquid structures are still possible, depending upon how the coordination polyhedra (CP) are linked. These differences are manifest at the level of the intermediate-range order (IRO), and this is affected by the anion polarization. Anion polarization controls the M–X–M bond angles [14] and, as a result, the degree of face-, edge- and corner-sharing between polyhedra. The signature of the IRO in the experimental structure factors is a prepeak, or first sharp diffraction peak (FSDP) at $\simeq 1$ Å^{-1}, indicative of ordering on a 5–10 Å length scale. On switching from the chloride to the bromide not only does the anion radius change, which is expected to change the preferred coordination number, but so also does the anion polarizability. It is of interest to see whether the (in principle) independent effects of these changes on the structure can be discerned by, for example, comparing the structure of a molten bromide (MBr_3) with a chloride ($M'Cl_3$) with the same radius ratio.

In this paper four bromide systems will be considered: $DyBr_3$, YBr_3, $LaBr_3$ and $CeBr_3$ for which the total neutron scattering structure factors have been measured by Wasse and Salmon [3,11]. These systems were chosen for the experimental study because the similar radii of the cation pairs $\{Y^{3+}, Dy^{3+}\}$ and $\{La^{3+}, Ce^{3+}\}$ would be expected to lead to similar liquid structures. By exploiting the differences in cation neutron cross-sections and this isomorphous assumption, *difference functions*, which, with particular relative scattering lengths, may approximate to partial structure factors, can be constructed. From comparison with chloride systems of similar radius ratio, we might expect the $LaBr_3$ and $CeBr_3$ ($\rho_{+-} = 0.77$) to be relatively high-coordinate ionic melts, like $LaCl_3$, and $DyBr_3$ ($\rho_{+-} = 0.67$) and YBr_3 ($\rho_{+-} = 0.66$) to form networks similar to $ScCl_3$, at the lower end of the band of stability of the six-coordinate 'step'. In terms of their crystal structures, both $LaBr_3$ and $CeBr_3$ adopt nine-coordinate UCl_3 structures, isomorphous with their chlorides, whilst both YBr_3 and $DyBr_3$ adopt six-coordinate BiI_3-like structures [15]. Although this structure is different to the YCl_3 structure adopted by the chlorides, both structures are based on MX_6 octahedra, differing only in the linkages.

2. Potential models and simulation details

2.1. Polarization

The polarization model includes dipoles induced on the anions only, following the simulation work on the metal trichlorides. Although some of the cations considered in the present work have appreciable polarizabilities (for example, $\alpha_{La^{3+}} = 7.673$ au [16]) the large size of these cations, coupled with large excess of anions, means that each cation tends to be symmetrically coordinated by a relatively large number of anions resulting in near-zero fields at the cation, and hence only small cation dipoles. Conversely, one expects the anions to have relatively low coordination numbers and so sit in asymmetric environments leading to significant dipole polarization effects.

The polarization part of the potential is based upon an explicit representation of the induced multipoles as variables, comparable to the ion positions, used to characterize the state of the system and its energy. The induced dipole on each ion, for a given configuration is obtained by minimization of the potential

$$U_{pol} = -\sum_{i,j}\left(\boldsymbol{\mu}_i \cdot \boldsymbol{T}^{(1)}(\boldsymbol{r}_{ij}) q_j f_{ij}(r_{ij}) + \frac{1}{2}\boldsymbol{\mu}_i \cdot \boldsymbol{T}^{(2)}(\boldsymbol{r}_{ij}) \cdot \boldsymbol{\mu}_j\right) + \sum_i k^i \mu_i^2 \tag{2.1}$$

with respect to all the dipoles $\{\boldsymbol{\mu}_i\}$. These self-consistent dipoles are the induced dipoles of the model and U_{pol} evaluated with these dipoles is the polarization energy associated with that configuration. The final term in the equation is a Drude-like representation of the energy required to polarize each ion and the force constant k^i is determined by the ionic polarizability (α^i):

$$k^i = \frac{1}{2\alpha^i}. \tag{2.2}$$

In equation (2.1), q^i is the formal ionic charge, and the $\boldsymbol{T}^{(n)}$-tensors are the normal charge–dipole and dipole–dipole interaction tensors:

$$T_\alpha^{(1)}(\boldsymbol{r}) = -r_\alpha / r^3 \qquad T_{\alpha\beta}^{(2)}(\boldsymbol{r}) = (3r_\alpha r_\beta - r^2\delta_{\alpha\beta})/r^5. \tag{2.3}$$

The r-dependence of the charge–dipole interaction is modified, to account for the short-range induction effects uncovered in electronic structure calculations [17, 18], by the factor $f_{ij}(r_{ij})$, which depends on the identities of the ions involved and which is a function of their separation. A suitable form for this function has been found to be

$$f_{ij}(r) = 1 - c^f \sum_{k=0}^{k_{max}^f} \frac{(b^f r)^k}{k!} \mathrm{e}^{-b^f r} \tag{2.4}$$

(as suggested by the Tang–Toennies dispersion 'damping' functions [19]). This function switches from the large-r value of 1 (meaning that the charge–dipole interaction regains pure Coulombic form in this limit) to $1 - c^f$ at $r = 0$ with a range determined by b^f. The parameters c^f and k_{max}^f allow for further flexibility in these functions to transfer effectively to quadrupole interactions [17, 18]. Since these are not our concern here we follow the metal trichloride work by setting $c^f = 1$ and $k_{max} = 4$.

To parametrize the polarization model we require both an anion polarizability and a set of anion–cation short-range damping parameters (SRDP), b^f. The dipole polarizability of the Br^- ion is taken as 30.0 au consistent with typical in-crystal alkali halide values [16] and the experimental refractive index of $LaBr_3$ [20]. Recent *ab initio* work [17, 18] has shown how

the SRDPs scale in a physically transparent manner from one system to another within a given stoichiometry with the sum of ion radii. Thus,

$$b^f = \frac{d_-^f}{\sigma_+ + \sigma_-} \tag{2.5}$$

where d_-^f is a property of the anion. d_-^f is obtained from the *ab initio* calculations by considering sets of specific distortions of nearest-neighbour cations about a central anion and fitting the short-range induced dipoles to equation (2.4). Furthermore, these calculations show that the scaling arguments hold for different halide ions [17, 18]. As a result of these considerations, the damping parameters used here are scaled from those used to reproduce the metal trichloride structures [7] and are given in table 1.

Table 1. Potential parameters for the MBr_3 systems scaled from the corresponding metal trichloride parameter sets.

Ion pair	a_{ij}/au	σ/Å	B_{ij}/au	C_6^{ij}/au	b/au
Br–Br	1.260	1.83	46.2	333.084	—
La–Br	2.439	1.42	18342.1	142.788	1.209
Ce–Br	2.439	1.40	16726.8	142.788	1.216
Dy–Br	2.439	1.22	7296.4	142.788	1.288
Y–Br	2.439	1.20	6653.9	65.064	1.296

2.2. Short-range parameters

The non-polarization aspects of the potential are given by pair potentials of Born–Mayer type:

$$u_{\mathrm{BM}}^{ij}(r^{ij}) = B^{ij}\mathrm{e}^{-a^{ij}(r^{ij})} + \frac{Q^i Q^j}{r^{ij}} - \frac{C_6^{ij}}{r^{ij\,6}} \tag{2.6}$$

where B^{ij} and a^{ij} represent the range and 'hardness' of the repulsive wall respectively, and C_6 is the dipole–dipole dispersion parameter. The short-range repulsion parameters are derived from those used to model the chlorides by rescaling in terms of the difference in anion radii ($\sigma_{\mathrm{Cl}^-} = 1.70$ Å compared with $\sigma_{\mathrm{Br}^-} = 1.83$ Å). Thus,

$$B_{\mathrm{MBr}} = B_{\mathrm{MCl}}\mathrm{e}^{a\,\Delta\sigma} \tag{2.7}$$

where $\Delta\sigma = \sigma_{\mathrm{Br}^-} - \sigma_{\mathrm{Cl}^-}$. Table 1 lists the repulsion parameters derived in this manner along with the ion radii used. The hardness of the repulsive wall, a, is assumed constant throughout for all anion–cation pairs, and the same as that from the metal trichloride simulations.

The dispersion terms are included up to the dipole–dipole interactions and are parametrized from the bromide polarizability (30.0 au) coupled with *ab initio* cation polarizabilities [16], where available, using the Slater–Kirkwood formula [21]. The polarizabilities for the Dy^{3+} and Ce^{3+} ions are not available and so the dispersion parameters are derived assuming the same polarizability as the La^{3+} ion reflecting their closeness in the periodic table.

2.3. Simulation details

Simulations are performed on systems of 125 molecules (125 M^{3+} and 375 Br^- ions) at densities and temperatures corresponding to the experimental neutron scattering conditions: $LaBr_3$, 4.481 g cm^{-3} (1083 K); $CeBr_3$, 4.496 g cm^{-3} (1053 K); $DyBr_3$, 4.15 g cm^{-3} (1190 K); YBr_3, 3.45 g cm^{-3} (1213 K). Run times in excess of 100 ps are used in all cases. Ewald summations are used to treat the charge–charge, charge–dipole and dipole–dipole interactions.

Partial (Ashcroft–Langreth) structure factors $S_{\alpha\beta}(k)$, can be calculated both by directly averaging over the correlation functions of the Fourier components of the ion densities:

$$S_{\alpha\beta}(k) = (N_\alpha N_\beta)^{-1/2}\left\langle \sum_{i\in\alpha}\sum_{j\in\beta}\exp[\mathrm{i}\boldsymbol{k}\cdot\boldsymbol{r}_{ij}]\right\rangle \tag{2.8}$$

and also by Fourier transformation of the partial pair distribution functions (pdf):

$$S_{\alpha\beta}(k) = \delta_{\alpha\beta} + 4\pi n_0\sqrt{c_\alpha c_\beta}\int \mathrm{d}r\ (g_{\alpha\beta}(r)-1)r\frac{\sin(kr)}{k} \tag{2.9}$$

where c_α is the mole fraction of species α and n_0 is the ionic number density. At low k, the former method (when using $\boldsymbol{k}$-vectors commensurate with the simulation cell) gives a more reliable structure factor, since it is free of truncation errors. The functions displayed in the current work are obtained by combining the direct averages, for $k \leqslant 2$ Å^{-1}, with the Fourier transformed pdfs for larger k-values.

3. Comparison with experimental structure factors

The total (neutron-weighted) structure factor, for comparison with experiment, is given by

$$F(k) = b_{\mathrm{M}}^2 c_{\mathrm{M}}[S_{\mathrm{MM}}(k)-1] + 2b_{\mathrm{Br}}b_{\mathrm{M}}\sqrt{c_{\mathrm{Br}}c_{\mathrm{M}}}S_{\mathrm{MBr}}(k) + b_{\mathrm{Br}}^2 c_{\mathrm{Cl}}[S_{\mathrm{BrBr}}(k)-1] \tag{3.1}$$

where b_α is the coherent neutron scattering length of species α. Neutron scattering lengths are given in table 2 (reference [22]).

Table 2. The neutron scattering lengths [22] used in the calculations of the weighted structure factors.

Species	Br	Cl	I	La	Ce	Dy	Y	Sc
b/fm	6.795	9.5770	5.28	8.24	4.84	16.9	7.75	12.29

Approximations to the partial structure factors can be obtained from the experimental data by taking differences between structure factors for systems with very similar physicochemical properties. For example, Wasse and Salmon [11] have applied this principle to their neutron scattering data for LaX_3 and CeX_3 (X = Cl, Br, I), noting that the ionic radii of La and Ce are very similar. They assume that $LaBr_3$/$CeBr_3$ and YBr_3/$DyBr_3$ are isomorphous pairs, differing only in the neutron scattering lengths of the cations.

If, for example, $S_{\mathrm{LaLa}}(k) = S_{\mathrm{CeCe}}(k) = S_{\mathrm{MM}}(k)$ and $S_{\mathrm{LaBr}}(k) = S_{\mathrm{CeBr}}(k) = S_{\mathrm{MBr}}(k)$, then the first-order difference function $\Delta_{\mathrm{M}}(k)$, in terms of Ashcroft–Langreth structure factors, is given by

$$\Delta_{\mathrm{M}}(k) = F_{\mathrm{LaBr_3}}(k) - F_{\mathrm{CeBr_3}}(k) = K_{\mathrm{MM}}[S_{\mathrm{MM}}(k)-1] + K_{\mathrm{MBr}}S_{\mathrm{MBr}}(k) \tag{3.2}$$

where

$$\begin{aligned} K_{\mathrm{MM}} &= c_{\mathrm{M}}(b_{\mathrm{La}}^2 - b_{\mathrm{Ce}}^2) \\ K_{\mathrm{MBr}} &= 2b_{\mathrm{X}}\sqrt{c_{\mathrm{M}}c_{\mathrm{Br}}}(b_{\mathrm{La}} - b_{\mathrm{Ce}}). \end{aligned} \tag{3.3}$$

Note that the $S_{\mathrm{BrBr}}(k)$ partial structure factor is eliminated. Using tabulated scattering lengths for La^{3+}, Ce^{3+} and Br^- [22] (table 2) gives values for K_{MM} of 111.2 mb and K_{MBr} of 200 mb showing that the $S_{\mathrm{MBr}}(k)$ partial accounts for 64% of $\Delta_{\mathrm{M}}(k)$.

The cation–anion correlations can be removed by forming the difference function $\Delta F'(k)$ defined as

$$\Delta F'(k) = F_{\mathrm{LaBr_3}}(k) - [b_{\mathrm{La}}/(b_{\mathrm{La}} - b_{\mathrm{Ce}})]\Delta_{\mathrm{M}}(k) = K^*_{\mathrm{BrBr}}[S_{\mathrm{BrBr}}(k)-1] - K^*_{\mathrm{MM}}[S_{\mathrm{MM}}(k)-1] \tag{3.4}$$

where

$$K^*_{\mathrm{MM}} = b_{\mathrm{La}} b_{\mathrm{Ce}} c_{\mathrm{M}}$$
$$K^*_{\mathrm{BrBr}} = b^2_{\mathrm{Br}} c_{\mathrm{Br}}. \tag{3.5}$$

Table 3 lists the weightings of the partial structure factors in the two difference functions for the two pairs of metal tribromides considered here. It can be seen that, in both cases, the difference function has a substantial weighting from both partials. This contrasts with the situation in the chlorides where, because of the different anion scattering lengths, the difference function approximates to a single partial. Nevertheless, as we shall see, even the elimination of one partial provides a useful additional comparison between experimental and simulated data.

Table 3. Relative weightings of the three partial structure factors making the two difference functions (equations (3.2) and (3.4)).

	$\Delta_{\mathrm{M}}(k)$		$\Delta F'(k)$	
	La/Ce	Y/Dy	La/Ce	Y/Dy
S_{MBr}	64	49	0	0
S_{BrBr}	0	0	78	51
S_{MM}	36	51	22	49

3.1. $LaBr_3$ and $CeBr_3$

Figures 1(a) and 1(b) show the total structure factors for $LaBr_3$ and $CeBr_3$ compared with the experimental values [3, 11]. Also shown are the partial structure factors weighted by the concentrations and neutron scattering lengths (equation (3.1)). The shapes of the partial structure factors for the two systems are very similar, as follows from the similarity of the cation radii; the differences in the total structure factors arises from the different neutron scattering lengths. For $CeBr_3$ the Br–Br term is weighted more heavily with respect to the M–Br than is the case for $LaBr_3$. For both systems, the M–M partial makes only a small contribution to the total. Each system shows a weak prepeak, whose position seems to be determined by a cancellation of intensity between the M–M and M–Br partials.

Figures 2(a) and 2(b) show the difference functions $\Delta_{\mathrm{M}}(k)$ and $\Delta F'(k)$. In both cases the agreement with experiment is good both in terms of the peak positions and intensities. The figures also show the appropriately weighted contributions of the two remaining partial structure factors, as in equations (3.2) and (3.4), to indicate the degree of similarity between the two difference functions and individual partial structure factors. The $\Delta_{\mathrm{M}}(k)$ difference function largely reflects the $S_{\mathrm{MBr}}(k)$ partial function since, although the weighting of $S_{\mathrm{MM}}(k)$ is relatively large compared to the corresponding chloride functions, $S_{\mathrm{MM}}(k)$ is relatively featureless beyond the principal peak. As a result, the effect of $S_{\mathrm{MM}}(k)$ is primarily to reduce the depth of the principal peak in $\Delta_{\mathrm{M}}(k)$ compared with $S_{\mathrm{MBr}}(k)$. The weightings of $S_{\mathrm{MM}}(k)$ and $S_{\mathrm{BrBr}}(k)$ in $\Delta F'(k)$ are such that this function is very heavily dominated by $S_{\mathrm{BrBr}}(k)$. Indeed, figure 2(b) shows that the contribution of $S_{\mathrm{MM}}(k)$ is only significant in the region of the principal peak where the difference in position of the main peaks in $S_{\mathrm{MM}}(k)$ and $S_{\mathrm{BrBr}}(k)$ leads to a slight shift of the main peak in $\Delta F'(k)$, with respect to that in $S_{\mathrm{BrBr}}(k)$, to a slightly smaller scattering angle.

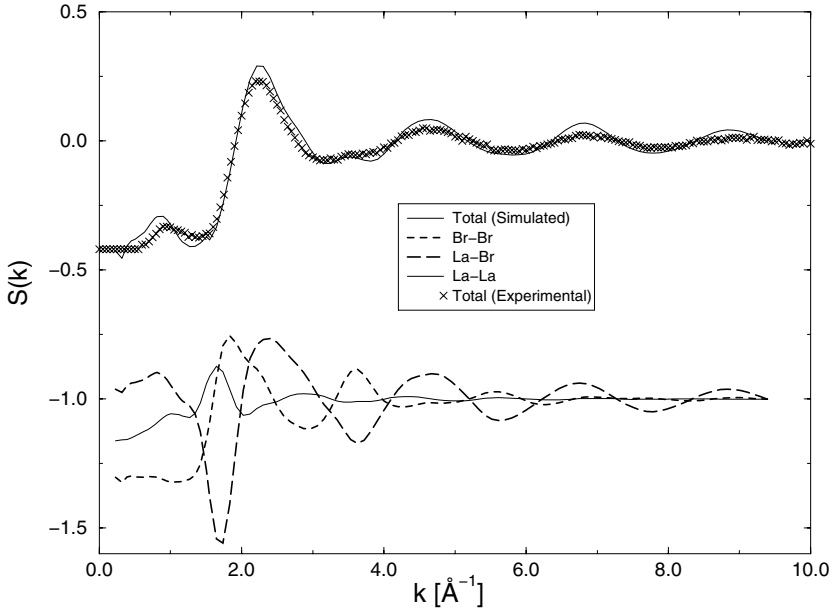

(a)

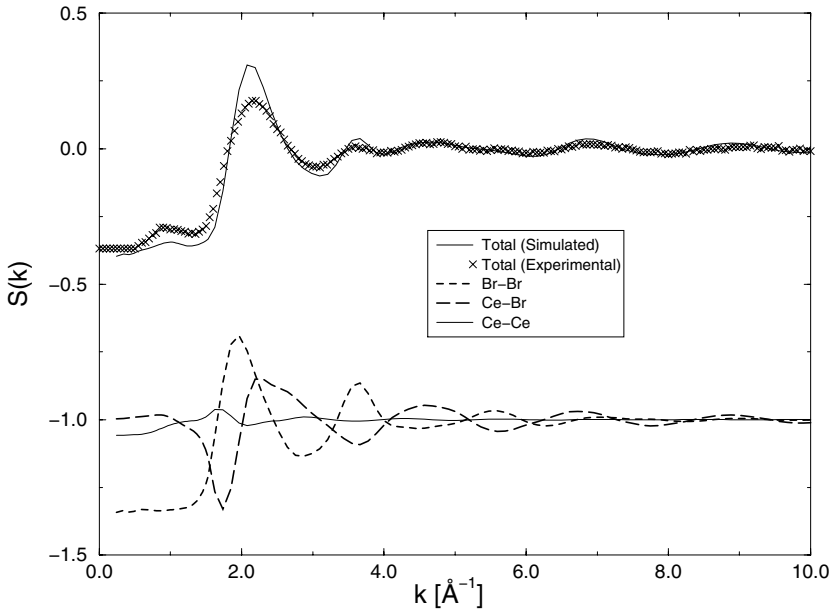

(b)

Figure 1. Simulated total structure factors (solid line) compared with experiment (×: reference [11]) for (a) $LaBr_3$ and (b) $CeBr_3$. The lower set of curves are the weighted contributions of the three partial structure factors to the simulated total.

3.2. YBr_3 and $DyBr_3$

Figures 3(a) and 3(b) show the total structure factors for YBr_3 and $DyBr_3$ with the lower panels showing the neutron-weighted partial structure factors. Again, the agreement with experiment

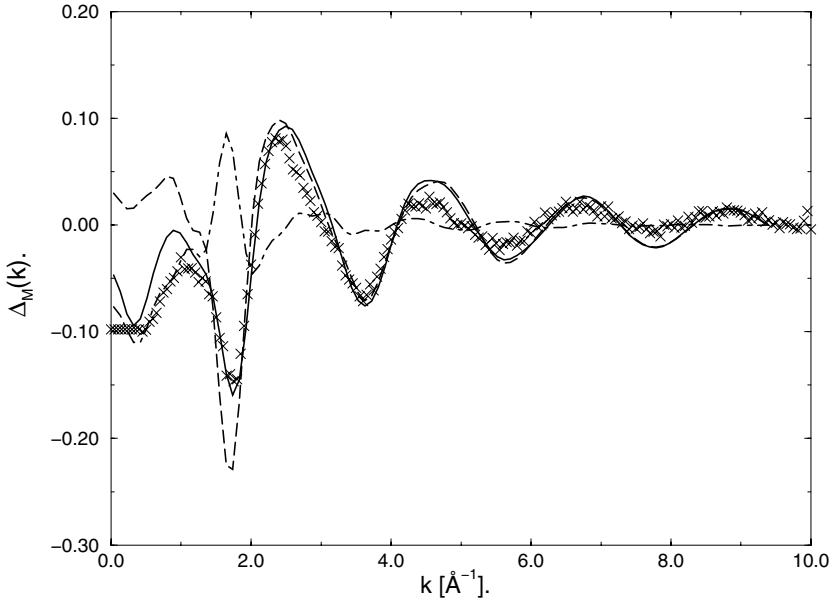

(a)

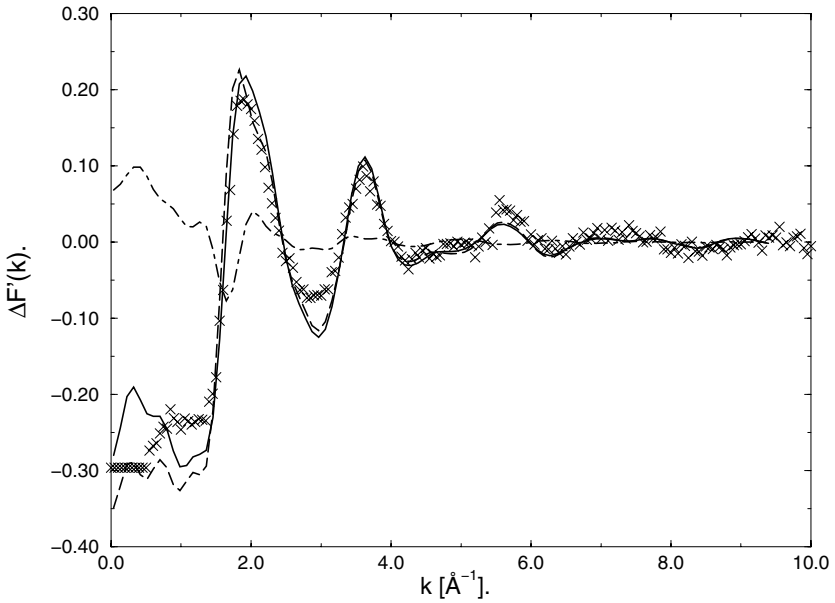

(b)

Figure 2. Difference functions for the $CeBr_3/LaBr_3$ isomorphous pair. (a) $\Delta_M(k)$. Key. ×: experiment [11]; solid line: simulation; dashed line: weighted $S_{MBr}(k)$ contribution; dot–dashed line: weighted $S_{MM}(k)$ contribution. (b) $\Delta F'(k)$. Key. ×: experiment [11]; solid line: simulation; dashed line: weighted $S_{BrBr}(k)$ contribution; dot–dashed line: weighted $S_{MM}(k)$ contribution.

is good for both systems, particularly in terms of the peak positions, though the intensity of the prepeak appears to be exaggerated. The pattern of intensity in the Y and Dy systems is very different to that seen in La and Ce, especially in the region of $2.5 \rightarrow 4$ Å^{-1}, and this

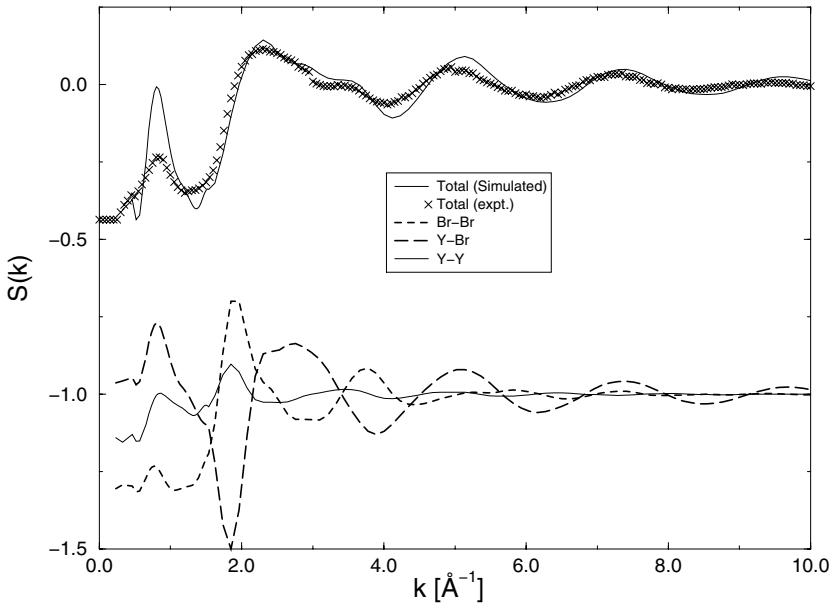

(a)

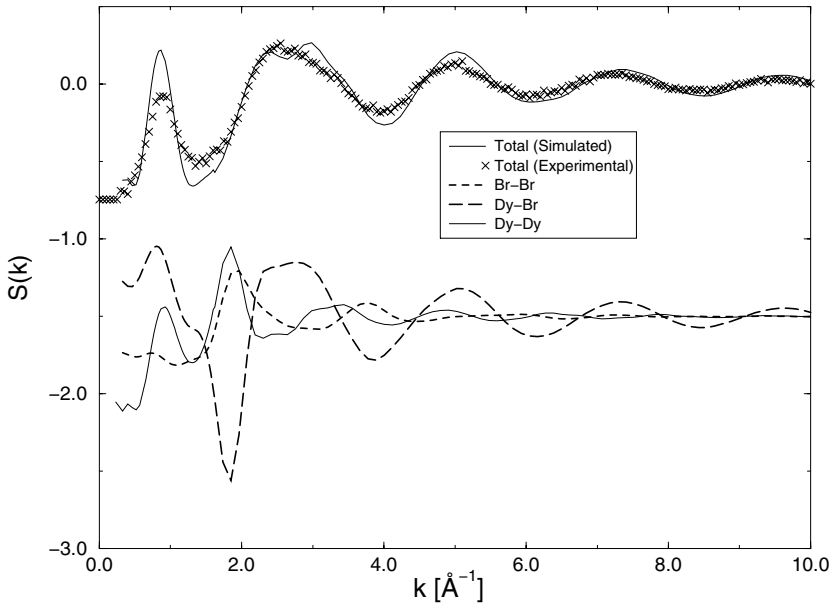

(b)

Figure 3. As figure 1 but for (a) YBr_3 and (b) $DyBr_3$.

is not simply an artifact of the change in scattering lengths; it indicates a significant change in the short-range order. As can be seen from an examination of the calculated partials in the two cases, for Dy and Y, the principal peaks in the cation–cation and anion–anion partials and the minimum in the cation–anion term occur at very similar positions ($\sim$2.0 Å^{-1}), so strong cancellation occurs in the total structure factor, leaving only the broad maximum at

2.5 → 4 Å^{-1} to which the cation–anion partial contributes most strongly. For La and Ce, these first peaks are not coincident to the same degree, so the total structure factor has a true principal peak at ∼2 Å^{-1}. As we shall see below, these differences reflect the fact that the La and Ce bromides belong to the high-coordination-number structural 'step' whereas the Y and Dy systems are roughly six-coordinate.

Note too that the prepeak has become very prominent in both the experimental and simulated structure factors. Contrary to the large-cation cases, La and Ce, the prepeak is seen to arise from a distinctive feature in the partial structure factors which is particularly prominent in the M–M and M–Br partials. The prepeak in the simulated pattern is narrower and shifted to slightly higher k than in the experimental structure factor. It is likely that this is attributable to system size effects, since the length scale of the intermediate-range order indicated by the prepeak position (∼8 Å) is only about one third of simulation cell length, and in similar studies of $ScCl_3$ [9] a broadening and down-shifting of the prepeak position on increasing the cell size was observed. It is also true that the low-k region is a difficult one on which to obtain reliable experimental information: a measure of such uncertainties can be gained by comparing the two experimental structure factors for YCl_3 [6, 23] which are very similar for $k > 1.5$ Å^{-1} but rather different at lower k.

Figures 4(a) and 4(b) show the difference functions $\Delta_M(k)$ and $\Delta F'(k)$ for YBr_3 and $DyBr_3$ compared to experiment. Again, the agreement with experiment is very good. However, the relative weightings of the two partials are, in both cases, approximately equal and, as a result, these difference functions are certainly not dominated by a single partial function. For $\Delta_M(k)$ the principal peak, at ≃2 Å^{-1}, is massively overdamped with respect to the corresponding peak in $S_{MBr}(k)$ by the contribution from the corresponding peak in $S_{MM}(k)$. Furthermore, the appearance of the FSDP in $\Delta_M(k)$ is heavily dominated by the contribution from $S_{MM}(k)$. However, as for $LaBr_3$ and $CeBr_3$, the relatively featureless nature of $S_{MM}(k)$ beyond the principal peak means that $\Delta_M(k)$ does largely reflect $S_{MBr}(k)$ at high scattering angle. Analogous comments apply to $\Delta F'(k)$ (figure 4(b)) with the intensity and position of the principal peak significantly shifted from that of the pure $S_{BrBr}(k)$ partial function by the considerable contribution from $S_{MM}(k)$.

As we noted in studies of the chlorides [7], it seems to be easier to demonstrate good agreement between a calculated partial structure factor and an experimental difference function than with a total structure factor. The total structure factor is *very* sensitive to the cancellation between oscillating features in the partials, as witnessed, for example by the way the partials contribute to the first peaks and also to the high-k structure in figures 1 and 3. Hence small errors in the correlation lengths which are barely visible in the partials have a big effect on the overall appearance of the total.

3.3. Isomorphisms between different halide systems

As we remarked in the introduction it is of interest to examine the extent to which the structures of bromide systems resemble those of chlorides with roughly the same radius ratio. One way of making this comparison is to combine the partial structure factors for the supposedly isomorphous chloride system with the appropriate neutron scattering lengths for the bromide and calculate a total structure factor which, under a uniform scaling of the scattering vector to allow for the difference in size of bromide and chloride ions, is compared with the experimental bromide structure factor.

Figure 5(a) shows the results of this procedure for YBr_3 ($\rho_{+-} = 0.66$) constructed from both the partial structure factors for $ScCl_3$ ($\rho_{+-} = 0.66$), which might be expected to be isomorphous, and those for $CeCl_3$ ($\rho_{+-} = 0.82$), which might not. The $ScCl_3$ ($CeCl_3$) partials

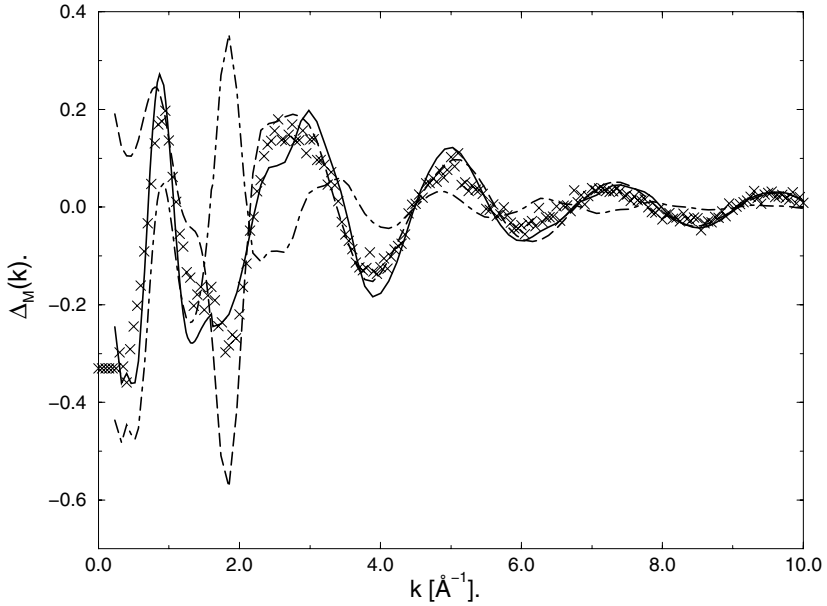

(a)

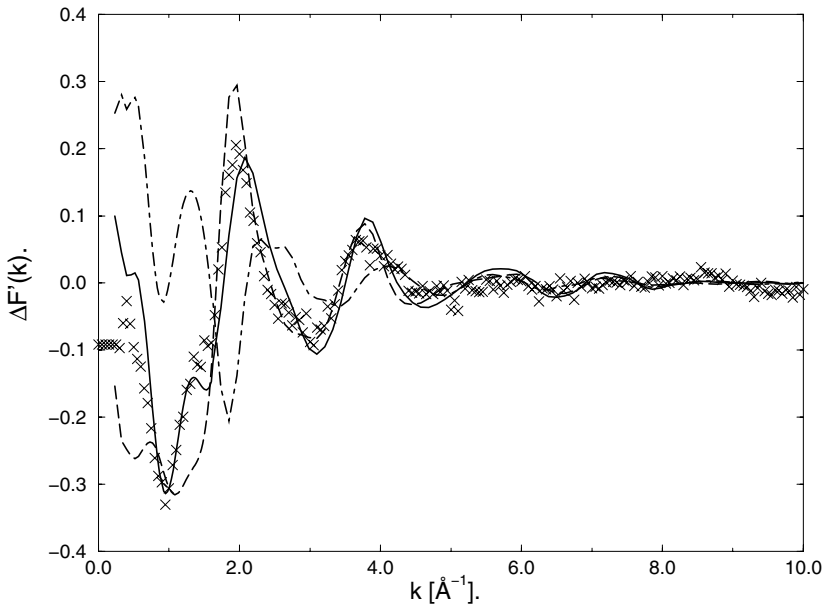

(b)

Figure 4. As figure 2 but for the $DyBr_3/YBr_3$ isomorphous pair.

are weighted by the appropriate scattering lengths for YBr_3 and the scattering vector of the chloride system is multiplied by 0.93, which is the ratio of chloride to bromide ion radii used in the simulation potentials.

The overall agreement between the $ScCl_3$-derived total structure factor and the YBr_3 experimental curve is excellent for, and beyond, the principal peak both in terms of the peak

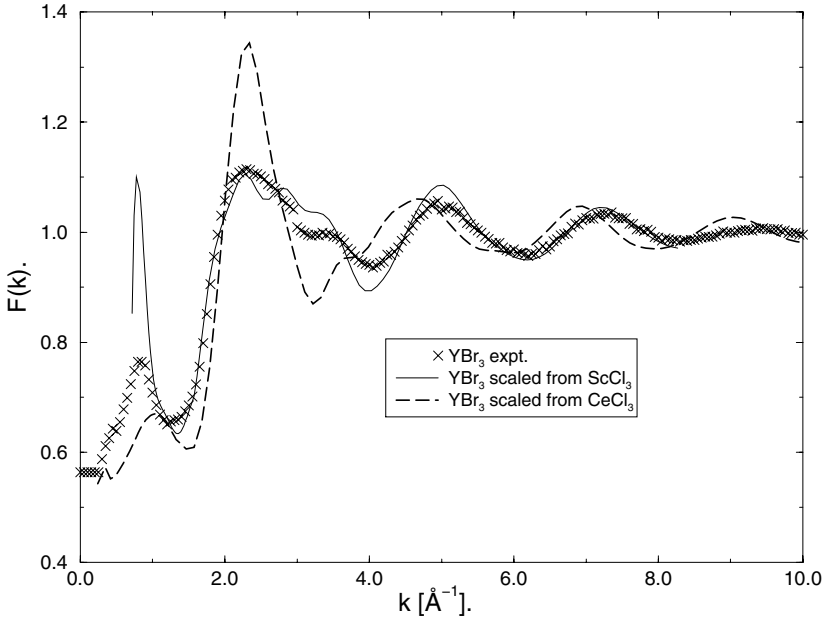

(a)

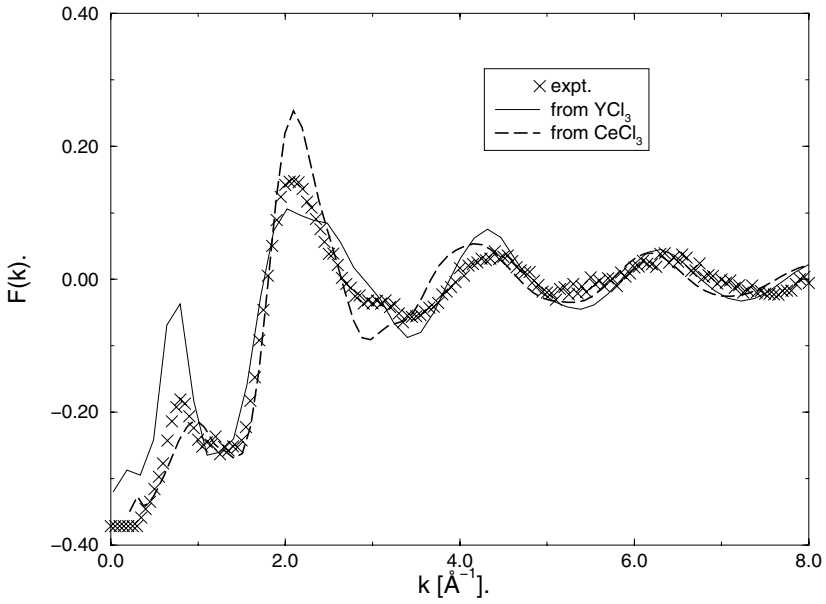

(b)

Figure 5. Total structure factors obtained from simulated partial functions using the scaling procedure in the text for (a) YBr_3, (b) CeI_3

positions and intensities. Furthermore, the corresponding agreement with the $CeCl_3$-derived curves is relatively poor. The comparison therefore suggests a structural similarity between $ScCl_3$ and YBr_3 and marked difference from the $CeCl_3$ structure. The most notable discrepancy between the YBr_3- and $ScCl_3$-derived structure factors is that the calculated prepeak is much

sharper than the experimental one (by even more than for the directly simulated YBr_3 structure factor), though its position is quite good. Again, we would suggest that this would be improved in simulations on larger samples.

Given the success of the above procedure, it is tempting to extend the analysis to molten metal tri-iodides for which experimental structure factor information is available for LaI_3, CeI_3 [11] and ScI_3 [5]. Figure 5(b) shows the experimental total structure factor for LaI_3 ($\rho_{+-} = 0.65$ using $\sigma_{I^-} = 2.16$ Å) compared to the functions scaled from YCl_3 and $CeCl_3$ respectively. The YCl_3-derived function is in good agreement with the LaI_3 experimental function for the principal peak and larger scattering angles. The $CeCl_3$-derived function is, as would be expected from the scaling arguments, a much poorer fit to the LaI_3 data. This is an interesting example, showing that the structure type can change for a given cation. $CeCl_3$ and $CeBr_3$ clearly belong to the high-coordination-number structure type whereas this good agreement of the LaI_3 structure factor with the scaled YCl_3 data shows that it belongs in the same structure type as the approximately octahedrally coordinated systems. Furthermore, the clear implication is that LaI_3 (and also CeI_3) undergoes a considerable structural transformation on melting resulting from a significant change in coordination number from the crystalline 8 + 1 coordination ($PuBr_3$ structure) to a liquid structure based around six-coordinate species. Indeed, the experimentally determined liquid coordination numbers support such a drop in coordination number [11] as does the relatively large volume change ($\Delta V/V \simeq 24\%$).

The radius ratio for ScI_3 ($\rho_{+-} = 0.52$) is quite small; it is intermediate between those of $ScCl_3$ and $FeCl_3$ amongst the chlorides. This is the region in which the melt coordination number of the chlorides switches from about 6 to 4. The comparisons show that the structure factor of ScI_3 is somehow intermediate between the scaled $ScCl_3$ and $FeCl_3$ functions, but the overall agreement is not as good as for the cases discussed above.

These comparisons suggest that the melt structures of the trivalent metal halides are predominantly determined by the radius ratio. In the introductory section we noted that our simulation potentials for the bromides were 'transmuted' from those for the chlorides by changing the anion radius *and* the polarizability. It would appear from the dominant influence of the radius ratio that the change of polarizability has had little effect. However, this may be an oversimplified view, as the magnitude of the charge-induced dipole is affected by the distance of closest approach of the cation and anion (approximately cubed) as well as by the magnitude of the polarizability and the larger size of the heavier halides will counteract the tendency to an increase in polarization effects arising from the increase of polarizability. Indeed, the ratio of the polarizability to the ionic radius cubed for the halide ions is roughly constant. Hence, the correct view may be that the increase in polarizability has served to maintain a similar relationship between ion size and polarization effects in the different halide series.

4. Real-space structures

4.1. Comparison of radial distribution functions

By Fourier transformation of the experimental structure factor, $F(k)$, the neutron-weighted radial distribution function may be obtained:

$$G(r) = \frac{1}{2\pi^2 n_0}\int_0^\infty \mathrm{d}k\, k\frac{\sin(kr)}{k}F(k)$$
$$= b_M^2 c_M^2(g_{MM}-1) + 2b_{Br}b_M c_{Br}c_M(g_{MBr}-1) + b_{Br}^2 c_{Br}^2(g_{BrBr}-1). \qquad (4.1)$$

The experimental and calculated values for this quantity are compared in figure 6 for the isomorphous pairs $LaBr_3$–$CeBr_3$ and YBr_3–$DyBr_3$ respectively. Also shown are the separate

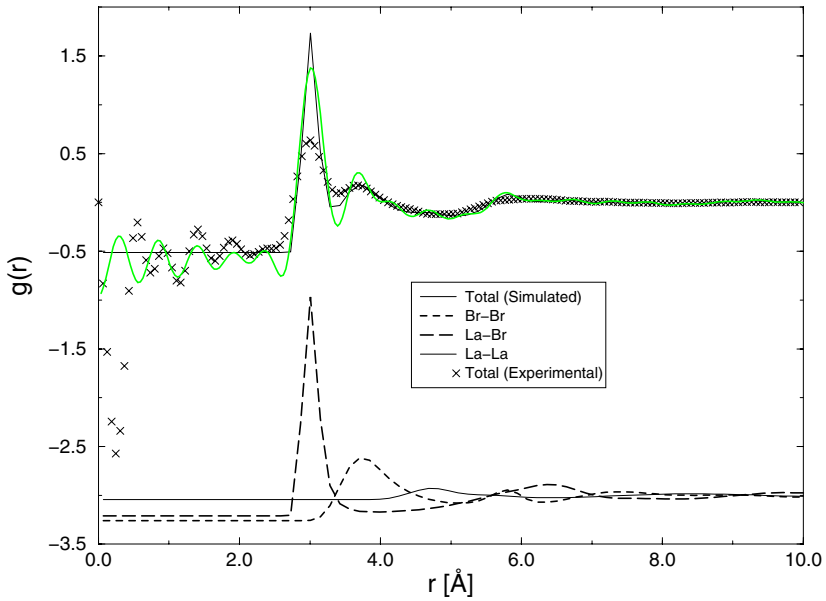

(a)

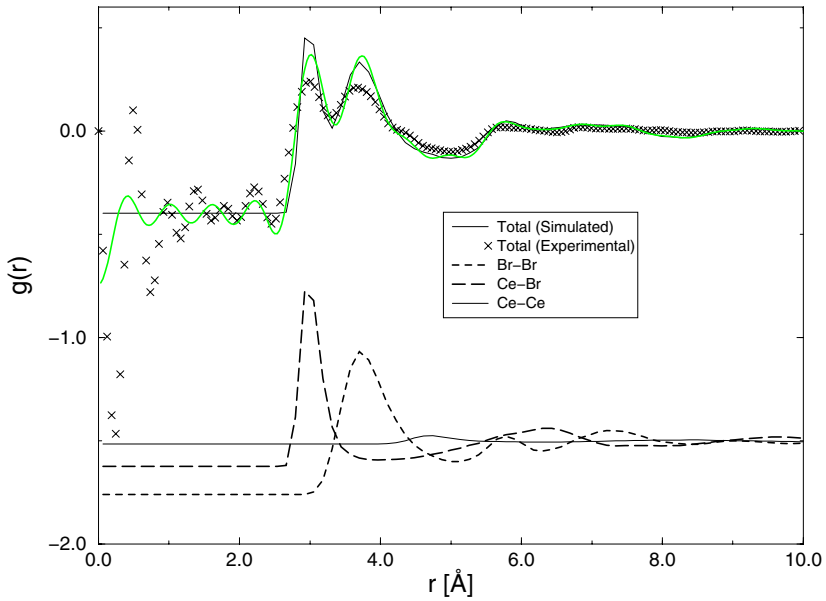

(b)

Figure 6. Radial distribution functions compared with the experimental transforms for (a) $LaBr_3$, (b) $CeBr_3$, (c) YBr_3 and (d) $DyBr_3$. Key: upper curves: ×: experiment; solid lines: simulated total functions calculated directly from the partial rdfs; light solid lines: back-transforms of simulated total structure factors. Lower curves: weighted partial rdf contributions.

(This figure is in colour only in the electronic version, see `www.iop.org`)

radial distributions obtained from the simulation, with the weights with which they contribute in equation (4.1). Except for the width of the first peak of $G(r)$, which is considerably narrower in

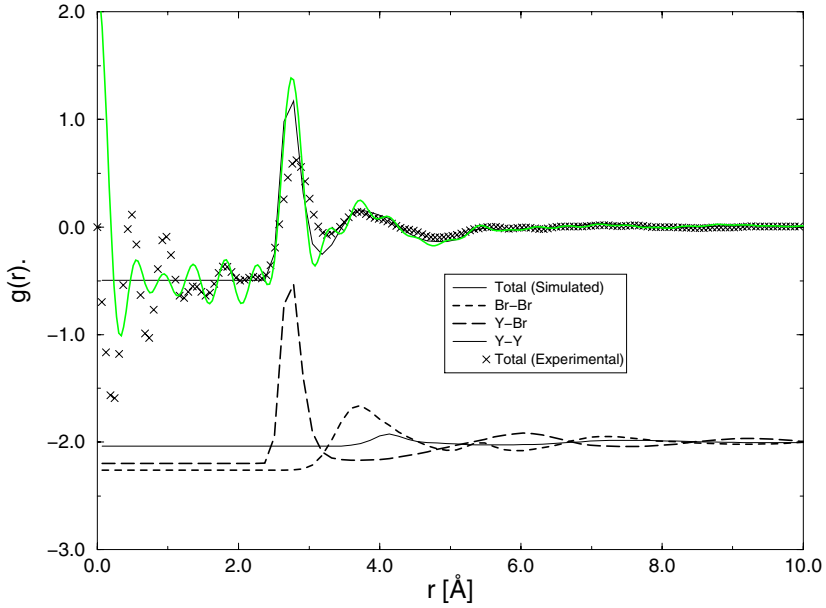

(c)

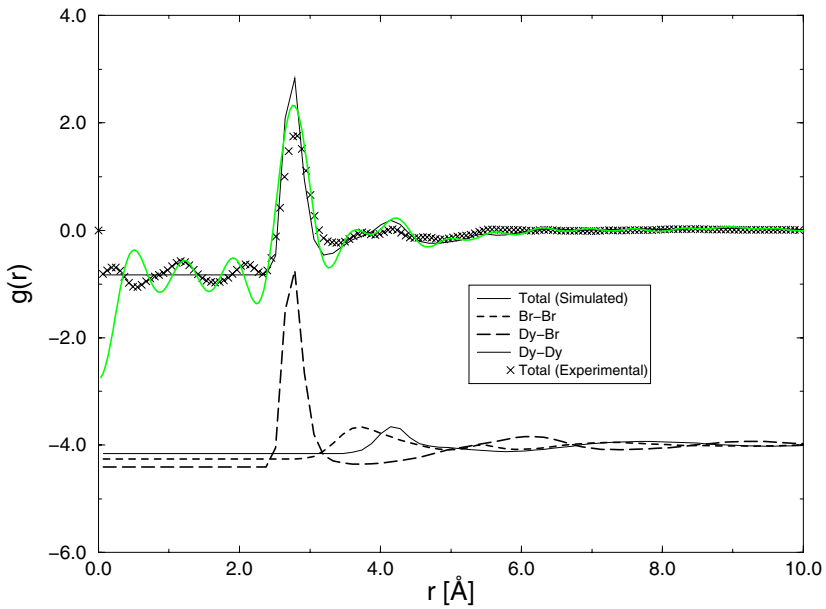

(d)

Figure 6. (Continued)

the simulation than in experiments, the agreement of the calculated and experimental quantities is good. The observation of greatest interest which emerges from this comparison is that, in favourable circumstances (scattering lengths), the experimental total rdfs do have features on the high-r side of the second peak in $G(r)$, which correspond to the first peak of the metal–metal rdfs. Such a feature can clearly be seen in the $DyBr_3$ and $CeBr_3$ cases. The position of

the M–M peak relative to the Br–Br is an important indicator of the nature of the links between the coordination polyhedra surrounding the cations [14, 24]. Note that the distance between these peaks is larger in the Ce case than in the Dy case (and also in La relative to Y in the simulated rdfs), whereas the absolute position of the first peak in g_{BrBr} is very similar for all systems. On the other hand, the greater separation between the first peak of g_{MBr} and g_{BrBr} in YBr_3 and $DyBr_3$ relative to $LaBr_3$ and $CeBr_3$ simply reflects the smaller cation size, and hence the smaller radius of the first coordination shell.

The most notable difference between the experimental and simulated distribution functions (figures 6(a)–6(d)) lies in the width (height) of the first peak. For all four systems the first peak in $G(r)$, attributable entirely to the anion–cation partial, is significantly too sharp. In part, this problem is caused by the truncation of the experimental data in order to perform the Fourier transform in equation (4.1). This is illustrated in figure 6(a) where, in addition to the simple linear combination of rdfs indicated by equation (4.1) we show a $G(r)$ obtained by Fourier transformation of the *simulated* $F(k)$ but with the reciprocal-space integral truncated at some upper limit k_c:

$$G(r) = \frac{1}{2\pi^2 n_0} \int_0^{k_c} \mathrm{d}k\, k \frac{\sin(kr)}{k} F(k). \tag{4.2}$$

The value of k_c is chosen so as to reproduce the period of the spurious low-r oscillations which are seen in the experimental $G(r)$ (no smoothing, or apodization has been performed in making this transform). It is clear that this procedure brings the simulated and experimental $G(r)$s into better agreement as regards the first peak height—indicating that the experimental procedure does broaden the first peak appreciably—however, it is also clear that it does not wholly remove the problem and that the simulated first peak remains too narrow. An analogous, although less pronounced, problem has already been observed for the metal trichlorides [7], and seems to reflect a shortcoming of the cation–anion repulsive potential.

That this problem appears to have been exacerbated, in passing from chlorides to bromides, can probably be traced back to the scaling procedures used to generate the short-range repulsion potential (section 2.2). The metal trichloride repulsion potential has simply been multiplied from the chloride potential by a constant factor to account for the increase in the anion radius, but the *shape* of the repulsion has not been changed. This would necessitate changing the repulsive wall 'hardness', i.e. also changing the parameter a in equation (2.1). The systematically greater sharpness of the first peak in $g_{\mathrm{MBr}}(r)$ relative to experiment is indicative of this repulsive wall being too steep. It is clear, therefore, that the M–Br repulsion should decay more slowly with separation than for the M–Cl ion pair, i.e. that a should be reduced. Such a trend is physically reasonable considering the greater volume of the Br^- anion.

In the interests of making the minimum number of changes to the potential, in order to stress that the structures of a very wide range of trihalides are accounted for by its generic form, we have not attempted to optimize the potential in this work. Future refinements should attempt to produce a potential which will account for the x-ray diffraction and EXAFS structural information, as well as the neutron data, and also for dynamical quantities such as the Raman frequencies [25].

4.2. Coordination number analyses

Anions are assigned to the first coordination shells of individual cations if they lie within a sphere of radius equal to the position of the first minimum in g_{MBr}. Table 4 lists the simulated mean cation–anion coordination numbers compared with experimental values obtained from

Table 4. Coordination numbers of M^{3+} cations in the molten tribromides.

	Mean CN		Coordination number distribution			
System	MD	Experiment	5	6	7	8
$LaBr_3$	7.1	7.40	0	17.5	58.4	23.4
$CeBr_3$	7.4	7.40	0	12.9	47.2	33.6
$DyBr_3$	6.2	6.10	4.0	74.4	20.0	1.6
YBr_3	6.2	6.00	5.6	74.4	17.6	2.4

$G(r)$. Despite the differences in widths of the first peaks of the rdfs noted above (figures 6(a)–6(d)), the agreement of the coordination numbers is good across the range of four systems. In the melt both sets of chlorides show higher mean coordination numbers compared with the corresponding bromides, consistent with the smaller Cl^- ion radius.

Both YBr_3 and $DyBr_3$ are dominated by six-coordinate species with a significant minority of seven-coordinate cations. $LaBr_3$ and $CeBr_3$ are mainly seven-coordinate with a large minority of eight-coordinate sites. With respect to the crystal structures, the coordination numbers for Dy and Y have increased slightly (from 6), and for La and Ce have decreased from 9 (perhaps better described as 6+3 for the UCl_3 structure). In the corresponding chlorides, these differences parallel the change in density on melting. For $DyCl_3$ and YCl_3 only a tiny volume change on melting is found, whereas for the systems melting from the UCl_3 structure, a significant increase in the volume $\sim$20% accompanies the coordination number decrease. The density data for the bromides do not appear to be available for making the same comparison. The local structures in the trivalent metal halides have often been discussed in terms of an ideal octahedral coordination polyhedron; from this perspective, the additional halides in the coordination shell (beyond 6) might be expected to be loosely coordinated outside the first coordination shell. The simulations do not support this interpretation. The first peaks in g_{MBr} are narrow and show no sign of subsidiary structure. Furthermore, a bond-angle analysis may be conducted on the ions in the first coordination shell and suggests that the coordination shell simply expands to accommodate the 'extra' halide ions in a uniform way. For YBr_3 and $DyBr_3$ the bond-angle analysis of the geometry shows the local coordination polyhedra to be mainly octahedra. For YBr_3, for example, the most intense peak in the bond-angle distributions for the Br–Y–Br triplets is at 81°, compared with 90° for an ideal octahedron. The difference between the observed bond angles and the ideal can be attributed to the distortions of the local octahedral coordination polyhedra in those coordination shells which contain an 'extra' ion at that instant. For $LaBr_3$ the Br–La–Br distribution peaks at 74°, and there is no evidence of secondary structure other than for this main peak.

The examination of the first coordination shells therefore suggests that for YBr_3 and $DyBr_3$ the cations are predominantly octahedrally coordinated with occasional ($\sim$20%) coordination shells containing an additional anion. Similar analyses of the first coordination shell in $ScCl_3$ [9], which has a slightly smaller cation:anion radius ratio, show that it is also predominantly octahedral, but with a significant number of five-coordinate cations and almost no seven-coordinate ones. Earlier, we showed that, despite this difference, the structure factors for YBr_3 and $DyBr_3$ closely resembled those obtained for $ScCl_3$. This suggests that all these systems fall into a class of octahedrally coordinated liquids with a common structure which is not strongly affected by small departures of the mean coordination number from 6. In $LaBr_3$ and $CeBr_3$ the average coordination number is greater than 7, only occasional cations are six-coordinate and the comparison of structure factors suggests that these liquids are qualitatively different from the octahedrally coordinated ones.

4.3. Inter-polyhedral linkages

Closer examination of the identities of ions involved, at some instant, in the coordination shells of more than one cation provides information on the linkages between the coordination polyhedra, and more insight into the structure types discerned above. Pairs of cations may be identified which lie within the range of the first minimum in the cation–cation partial radial distribution function. Bromide ions which bridge between such cations are those which lie within the coordination shells of *both* cations. Note that this type of analysis is most suited (for MX_3 systems) to those cases where the dominant cation coordination number is 6 (YBr_3 and $DyBr_3$ here). In these cases, it follows from the stoichiometry that the average anion coordination number is 2, so thinking of two cations linked by a single anion is natural. When the mean cation coordination number is significantly higher than 6, at least some of the anions have to be simultaneously coordinated to three or more cations which, as we shall see, causes qualitative changes in the liquid structure.

The linkages between the coordination polyhedra may characterized by calculating the number of anions simultaneously in the coordination shells of a given pair of cations—a single anion is interpreted as corner-sharing, two anions as edge-sharing and three as face-sharing. Table 5 lists the percentages of linkages for the YBr_3 and $DyBr_3$ systems. The data clearly show that the edge-sharing units predominate. The proportions of vertex-, edge- and face-sharing are greatly influenced by the anion polarization which leads to induced dipoles on the bridging anions when the M–Br–M bond is bent. These induced dipoles screen the repulsive M–M Coulombic interaction [14, 24], allowing a closer approach of the cations than would be the case if polarization effects were omitted, and increasing the proportion of edge- over vertex-sharing. In a series of systems with the same anion polarizability, the polarization effects become most important for the smallest cations. This effect can be seen in contrasting the positions of the first peaks of the MM and BrBr partial radial distribution functions for La/Ce with those for Y/Dy. It can be seen that the first peak of g_{MM} is much closer to that of g_{BrBr} in Y/Dy than in La/Ce. For $LaBr_3$ and $CeBr_3$ we can see that the proportion of edge-sharing units has decreased relative to that for Y/Dy. Note, however, that because in this case we are dealing with seven(/eight)-coordinate polyhedra, rather than octahedra, for which the number of edge-sharing connections is necessarily higher, the decrease in the proportion of edge-sharing units understates the influence of the diminished polarization effects

Table 5. Connectivity of MBr_n species.

	Connectivity		
System	Vertex	Edge	Face
$DyBr_3$	32.0	60.8	7.2
YBr_3	25.3	68.7	6.1

As well as influencing the distance of closest approach of the metal centres, these linkages determine the intermediate-range order in the melt. Using the figures in tables 5 we see that a Y^{3+} ion is connected, on average, to 6.2 Br^- ions. Through vertex-sharing connection, the Y^{3+} is therefore connected (on average) to 6.2×0.183 other Y^{3+} ions, through edge-sharing to an additional $6.2 \times 0.757/2$ and through face-sharing to a further $6.2 \times 0.061/3$, to give a total Y–Y 'coordination number' of 3.6. For Ce^{3+}, we obtain $7.4 \times (0.47 + 0.47/2 + 0.06/3) = 5.4$. Since this exhausts the number of Br^- ions to which the central cation is connected, these neighbours will lie within a well-defined shell, and all other Y^{3+} ions must lie at substantially greater distances away. If one imagines how to fill space with a network with such a low coordination

number as 3.6, one can see that there must necessarily be some substantial inhomogeneities (even a diamond lattice, with coordination number 4, has substantial holes). On the other hand, with a coordination number of 5.4 a more uniformly space-filling network can be envisaged. The signature of the greater inhomogeneity of the YBr_3 and $DyBr_3$ melts is the prominent prepeak which appears in the structure factor. As we have argued elsewhere [26, 27], the prepeak may be associated with the presence of voids in the spatial distribution of cations and the position of the prepeak is related to the inter-void separation. The most extreme example is $ScCl_3$ where the mean cation–cation 'coordination number' is close to 3; the voids are readily seen in snapshots of the atomic positions and result in an enormous prepeak at very low k [5].

Examination of molecular graphics snapshots of the ion positions in YBr_3 and $DyBr_3$ suggests chain-like structures constructed from connected edge-sharing octahedra [28]. To examine whether such observations are statistically significant we construct a pair distribution function to elucidate the structural correlations between the edge-sharing units. The four ions (two octahedral cations and two bridging anions) constituting an edge-sharing unit are identified and used to calculate the position of its centre (in an ideal edge-sharing unit a point equidistant between the two cations along the vector joining them). The centres are then treated analogously to the atomic positions and used to calculate the pair distribution function:

$$4\pi r^2 g_{\mathrm{EE}}(r) = \frac{V}{2N_{\mathrm{E}}} \sum_{i=2}^{N_{\mathrm{E}}} \sum_{j=1}^{j=i-1} \delta(|\boldsymbol{R}_i - \boldsymbol{R}_j| - r) \tag{4.3}$$

where N_{E} is the number of edge-sharing units in a configuration. Analogous functions can be constructed for the corner-sharing and face-sharing units if required along with the corresponding cross-correlations.

Figure 7 contrasts the edge–edge (EE) functions for $CeBr_3$ and YBr_3. The functions have been plotted versus r_{norm}, which is the inter-centre separation divided by the position of the

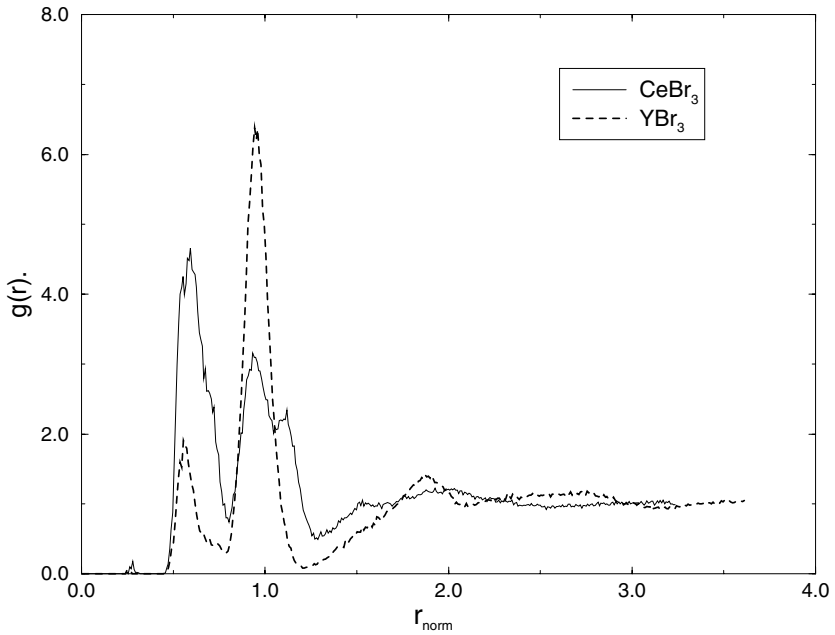

Figure 7. Edge–edge radial distribution functions for $CeBr_3$ (solid line) and YBr_3 (dashed line) as discussed in the text.

first peak in the cation–cation radial distribution function. A linear chain of edge-sharing units would give a peak in the distribution function close to $r_{norm} = 1$, and other arrangements of the edge-sharing units would also produce peaks at characteristic values of r_{norm}. It can be seen from the figure that the functions for YBr_3 and $CeBr_3$ differ from each other markedly. The $CeBr_3$ shows a large peak corresponding to adjacent edge-sharing units around the coordination polyhedron with a M–Br bond involved in two edge-sharing connections. Note that this unit involves a three-coordinate anion which, as we indicated above, will only be a common feature for liquids in which the cation coordination number is greater than 6. The $CeBr_3$ also shows peaks corresponding to other non-adjacent edge-sharing connections. The overall impression is that there is no strong constraint on the relative positions of these connections; one might think of coordination polyhedra simply being stacked together and the connections being made to accommodate the available anions. In YBr_3, on the other hand, a specific arrangement of non-adjacent edge-sharing connections seems to be strongly preferred. This arrangement may connect a series of polyhedra leading to a characteristic percolating chain structure.

Figure 8 shows a snapshot of the YBr_3 fluid structure, where the points mark the positions of the centres of the edge-sharing units and 'bonds' are drawn between them if their separation is less than 8.2 au—which corresponds to the position of the first maximum in g_{YY}. The figure highlights the existence of a percolating chain structure in which the cations are connected by edge-sharing. This structure is characteristic of the near-octahedrally coordinated trivalent

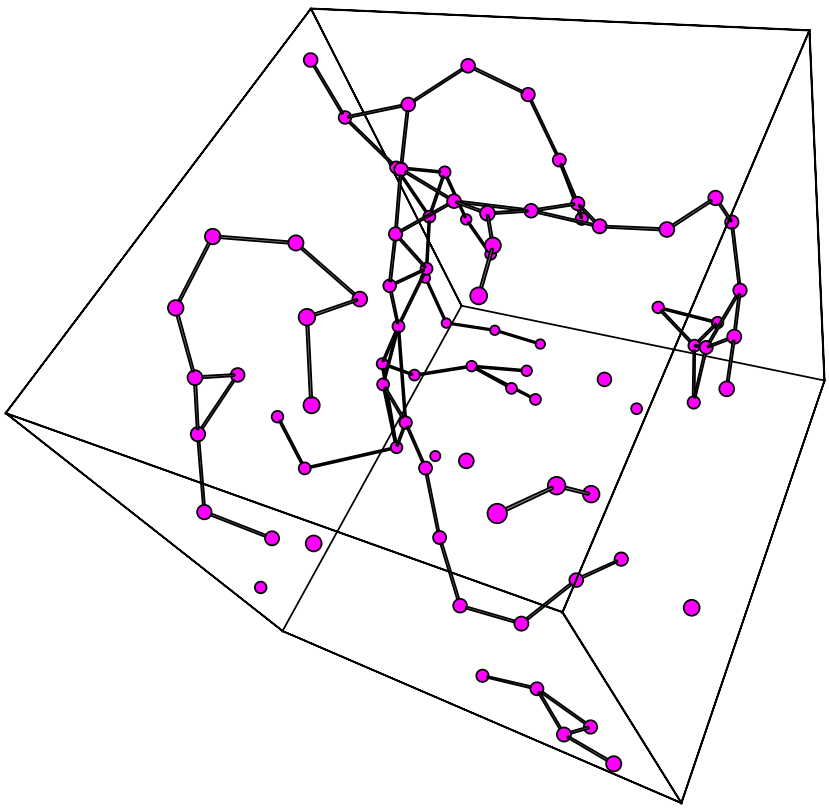

Figure 8. A molecular graphics 'snapshot' of the edge-sharing units in a single YBr_3 configuration highlighting the chain-like nature of the inherent structure.

metal halides that we have simulated and responsible for the pronounced IRO exhibited in the diffraction data.

5. Conclusions

The structures of the tribromides obtained with polarizable-ion potentials derived by systematically changing the anion radius and polarizability in the potentials previously used for the trichlorides seem to agree quite satisfactorily with the available experimental data. It would seem that the structures of the trihalide melts fall into three distinct structure classes, depending on the ratio of cation and anion radii and independent of the specific cation and anion involved. For a large radius ratio, a (7–8)-coordinate cation is found and the relative arrangements of these coordination polyhedra around neighbouring cations show no particular pattern; the polyhedra seem simply to pack together. The systems which form these liquids exhibit the nine-coordinate UCl_3 structure in the solid phase. For a wide range of intermediate radius ratios a family of structures based upon more-or-less six-coordinate cations arises. These approximately octahedral units exhibit a marked tendency to edge-share so as to form extended and cross-linked chains. This structural motif seems quite stable against variations in the actual mean coordination number from about 6.5 to 5.5. Most systems within this class exhibit the six-coordinate YCl_3 (or BiI_3) crystal structure, but some systems melt into it from higher-coordinate crystal structures, like the $(8 + 1)$-coordinate $PuBr_3$ structure. For still smaller radius ratios, quasi-molecular fluids based on four-coordinate cations are found, as in $AlCl_3$. Again, several of these systems melt from six-coordinate crystals. It would seem that the general rule [1, 2]—that ionic materials exhibit the same local structure across the melting transition—encounters a number of exceptions in the trihalides.

Acknowledgments

We gratefully acknowledge many helpful discussions and the free flow of information with Jonathan Wasse and Philip Salmon. MW thanks the Royal Society for a Research Fellowship. The work was supported by the EPSRC through grant GR/L/49369 and a studentship for FH.

References

[1] Enderby J E and Barnes A C 1990 *Rep. Prog. Phys.* **53** 85
[2] Tosi M P, Price D L and Saboungi M-L 1993 *Annu. Rev. Phys. Chem.* **44** 173
[3] Wasse J C 1998 *PhD Thesis* University of East Anglia
[4] Wasse J C and Salmon P S 1998 *Physica* B **241–243** 967
[5] Wasse J C and Salmon P S 1999 *J. Phys.: Condens. Matter* **11** 2171
[6] Wasse J C and Salmon P S 1999 *J. Phys.: Condens. Matter* **11** 9293
[7] Hutchinson F, Rowley A J, Walters M K, Wilson M, Madden P A, Wasse J C and Salmon P S 1999 *J. Chem. Phys.* **111** 1
[8] Hutchinson F, Walters M K, Rowley A J and Madden P A 1999 *J. Chem. Phys.* **110** 5821
[9] Hutchinson F, Wilson M and Madden P A 2000 unpublished
[10] Madden P A and Wilson M 1996 *Chem. Soc. Rev.* **25** 339
[11] Wasse J C and Salmon P S 1999 *J. Phys.: Condens. Matter* **11** 1381
[12] Saboungi M-L, Howe M A and Price D L 1993 *Mol. Phys.* **79** 847
[13] Akdeniz Z and Tosi M P 1992 *Proc. R. Soc.* A **437** 85
[14] Madden P A and Wilson M 2000 *J. Phys.: Condens. Matter* **12** A95
[15] Müller U 1993 *Inorganic Structural Chemistry* (Chichester: Wiley)
[16] Pyper N C 1991 *Adv. Solid State Chem.* **2** 223
[17] Ďemmer P, Wilson M, Madden P A and Fowler P W 1999 *J. Chem. Phys.* **111** 2038

[18] Domene C, Fowler P W, Wilson M and Madden P A 2000 *Chem. Phys. Lett.* at press
[19] Tang K T and Toennies J P 1984 *J. Chem. Phys.* **80** 3726
[20] Fukushima K and Iwadate Y 1996 *J. Alloys Compounds* **238** L1
[21] Slater J C and Kirkwood J G 1931 *Phys. Rev.* **37** 682
[22] Sears V F 1992 *Neutron News* **3** 26
[23] Saboungi M-L, Price D L, Scamehorn C and Tosi M P 1991 *Europhys. Lett.* **15** 283
[24] Takagi R, Hutchinson F, Madden P A, Adya A K and Gaune-Escard M 1999 *J. Phys.: Condens. Matter* **11** 645
[25] Dracopoulos V, Gilbert B, Borrensen B, Photiadis G M and Papatheodorou G N 1997 *J. Chem. Soc. Faraday Trans.* **93** 3081
[26] Wilson M and Madden P A 1998 *Phys. Rev. Lett.* **80** 532
[27] Barker D R, Wilson M, Madden P A, Medvedev N N and Geiger A 2000 *Phys. Rev.* E **62** 1427
[28] Hutchinson F 2000 *DPhil Thesis* University of Oxford